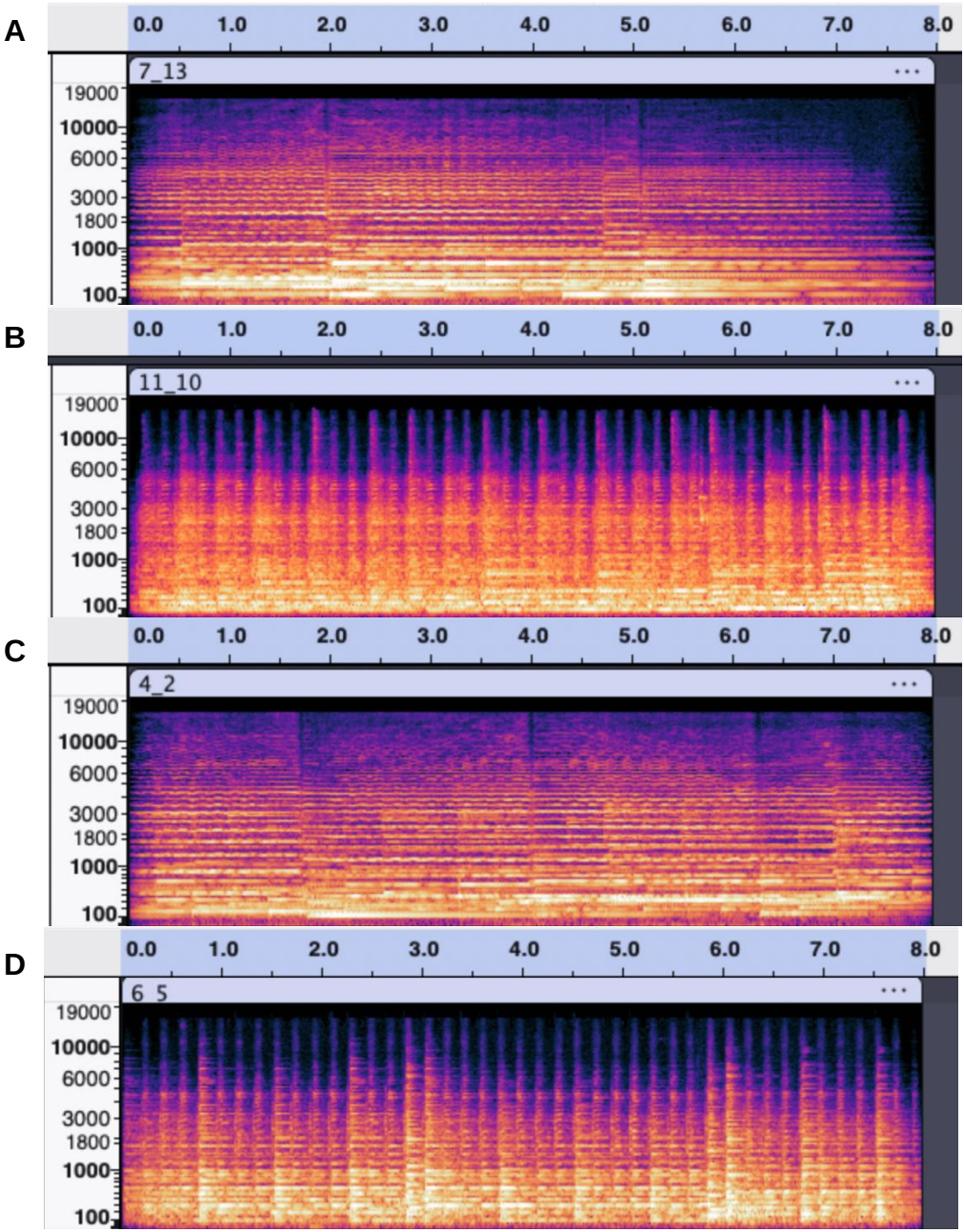

Figure 1. Spectrograms of four of the selected music stimuli with time (seconds) on horizontal scale and frequency (Hz) on vertical scale. **(A)** Negative valence stimulus that was identified as high arousal in the normed dataset but shows very little spectral flux and was therefore relabeled as low arousal. **(B)** Negative valence stimulus that was identified as high arousal in the normed dataset and shows high spectral flux and therefore retained its high arousal label. **(C)** Positive valence stimulus that was identified as low arousal in the normed dataset and shows low spectral flux and therefore retained its low arousal label. **(D)** Positive valence stimulus that was identified as high arousal for first half and low arousal for second half but shows high spectral flux throughout entire duration and was therefore relabeled as only high arousal.

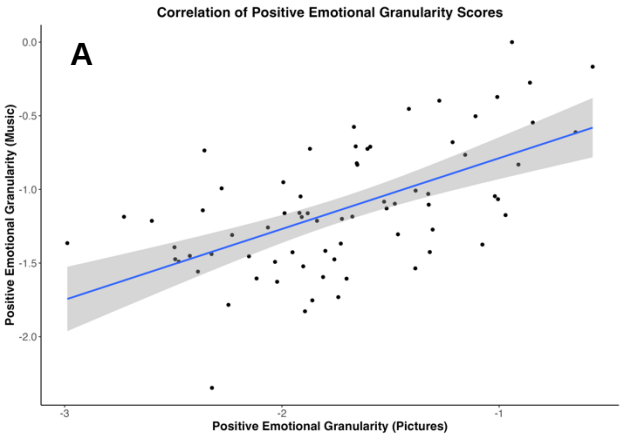

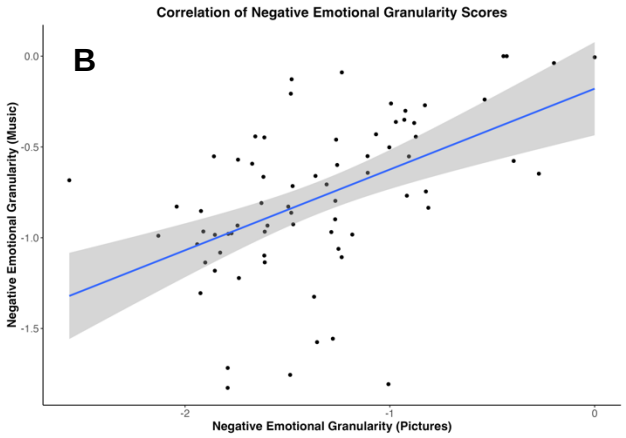

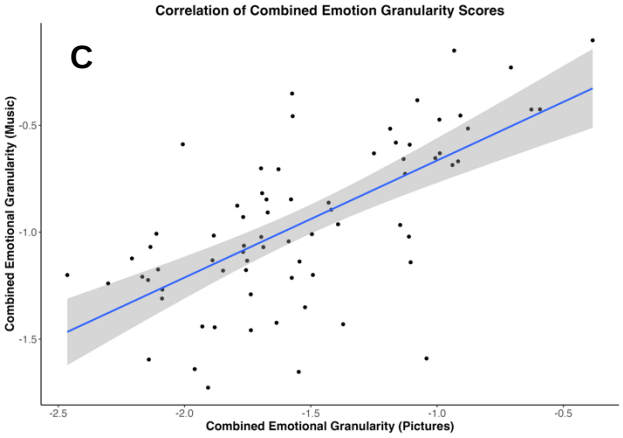

Figure 2. Study 1 scatter plots of correlations between granularity scores for positive emotions (**A**), negative emotions (**B**), and combined emotional granularity (**C**).

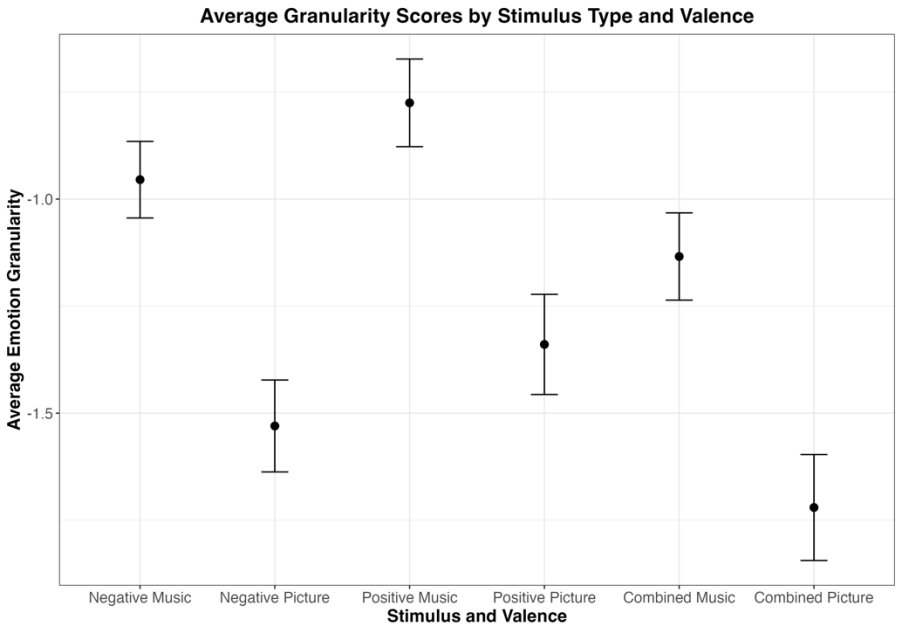

Figure 3. Study 1 average emotional granularity scores split by emotion valence (negative vs. positive) and stimulus type (picture vs. music). Error bars show 95% confidence intervals.

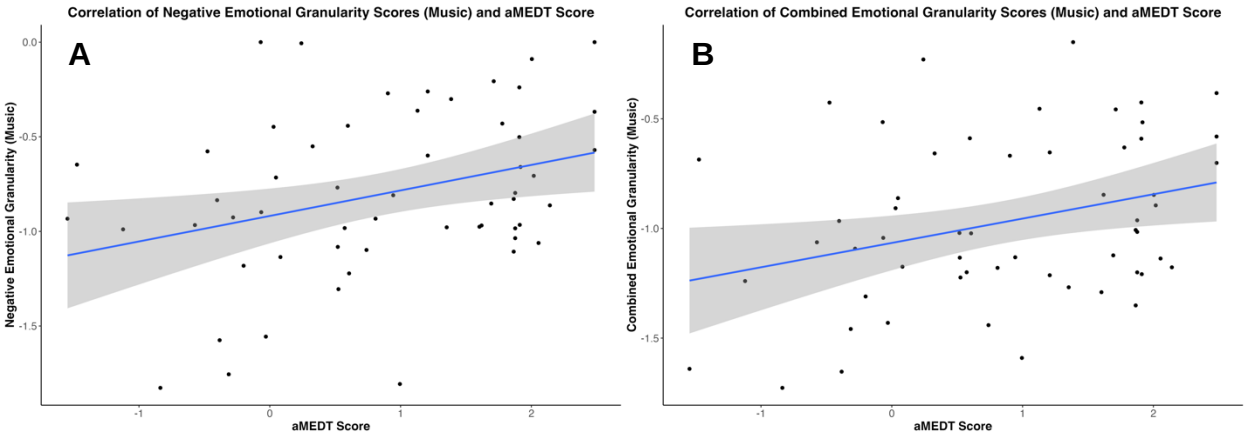

Figure 4. Study 1 scatter plot of significant positive correlations between negative **(A)** / combined (**B**) emotional granularity in response to music and musical emotion discrimination task score. **A.** $r(58) = .33$, $p = .014$
B. $r(58) = .31$, $p = .019$

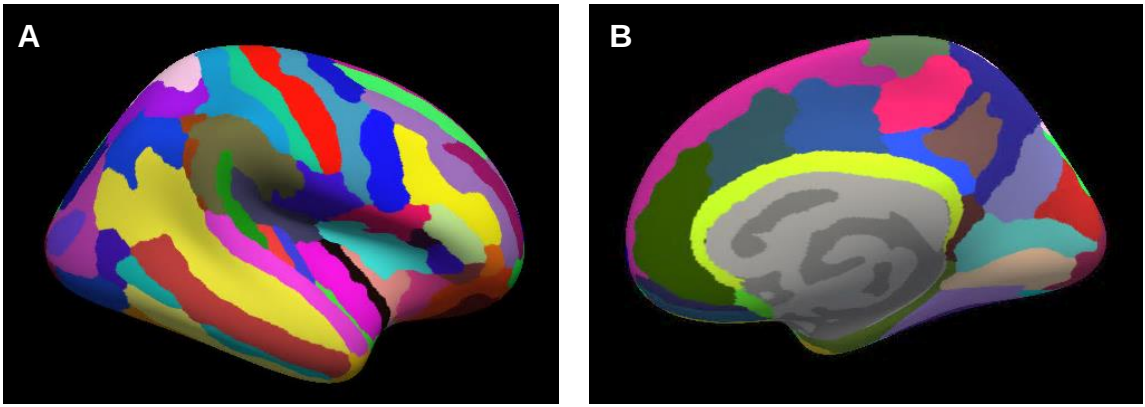

Figure 5. (A) Right hemisphere Freeview visualization of Destrieux atlas structural parcellation with 148 ROIs (default color labels). **(B)** Right hemisphere medial view of atlas visualized in **(A)**.

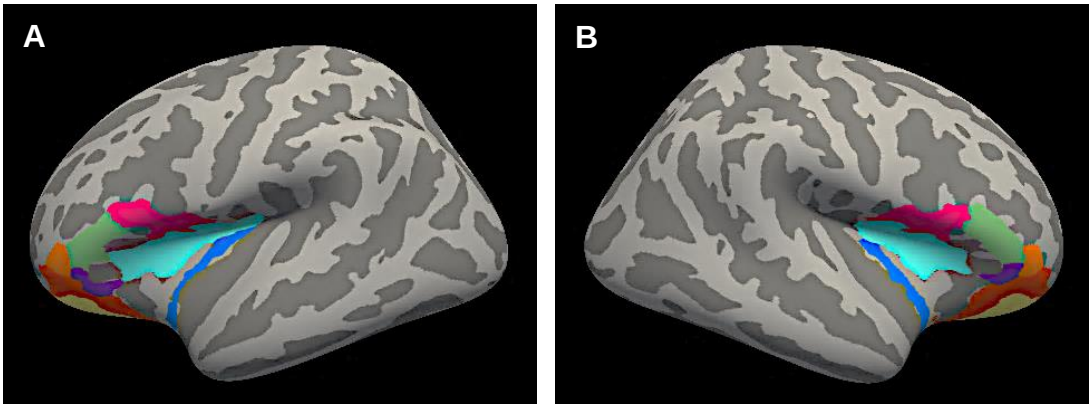

Figure 6. ROIs from Destrieux atlas: (1) Pars opercularis (BA45) (magenta), (2) pars triangularis (BA44) (green), (3) pars orbitalis (purple), (4) long insular gyrus and central sulcus of the insula (blue), (5) superior segment of the circular sulcus of the insula (cyan), (6) lateral orbital sulcus (orange), (7) orbital gyri (red), (8) H-shaped orbital sulci (yellow) of the left hemisphere **(A)** and right hemisphere **(B)**.

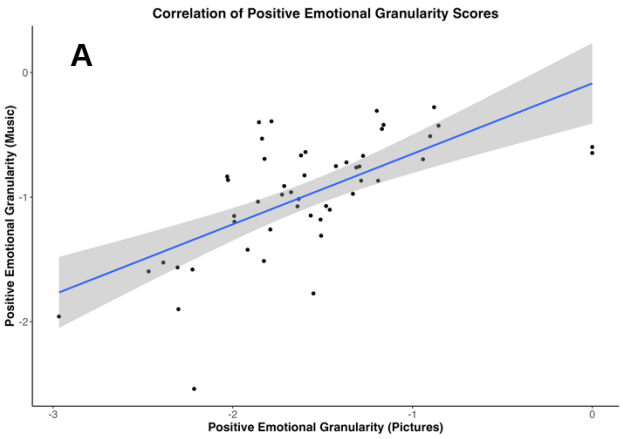

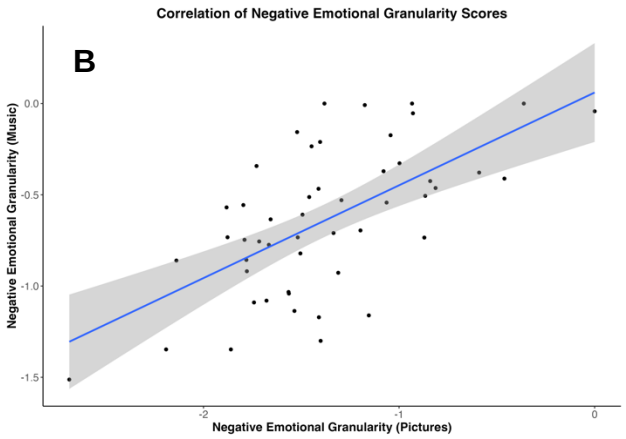

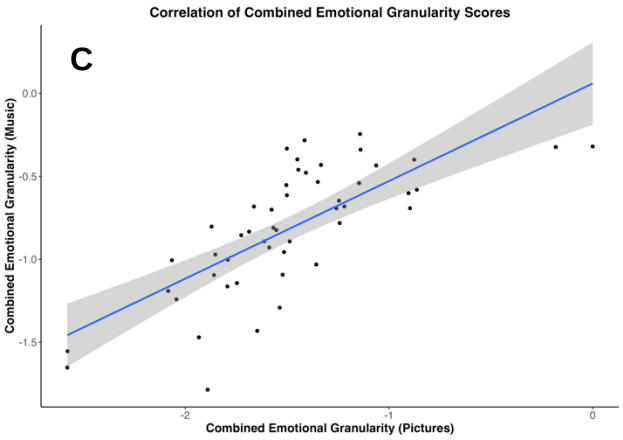

Figure 7. Study 2 scatter plots of correlations between granularity scores for positive emotions (**A**), negative emotions (**B**), and combined emotional granularity (**C**).

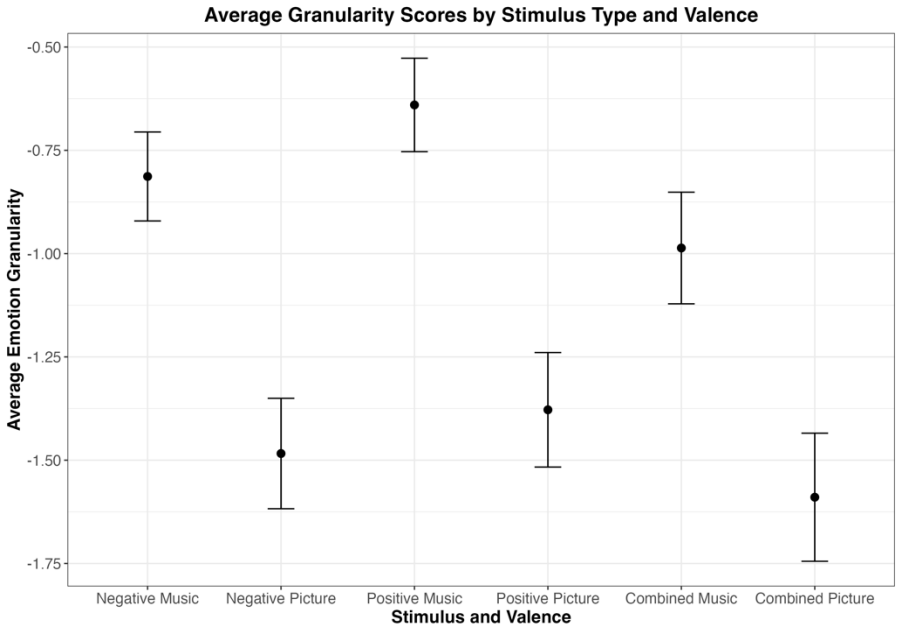

Figure 8. Study 2 average emotional granularity scores split by emotion valence (negative vs. positive) and stimulus type (picture vs. music). Error bars show 95% confidence intervals.

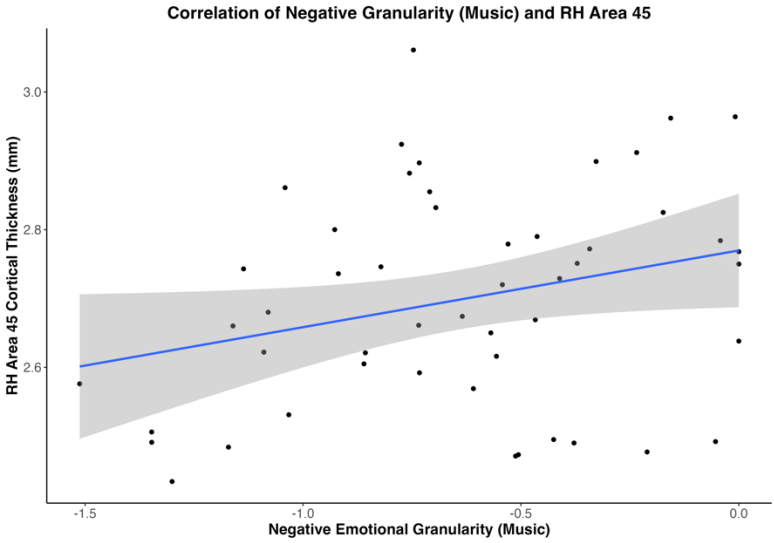

Figure 9. Study 2 scatter plot showing positive correlation between right hemisphere Area 45 (pars triangularis) cortical thickness and negative emotional granularity in response to music, $r(48) = .28$, $p = .047$.

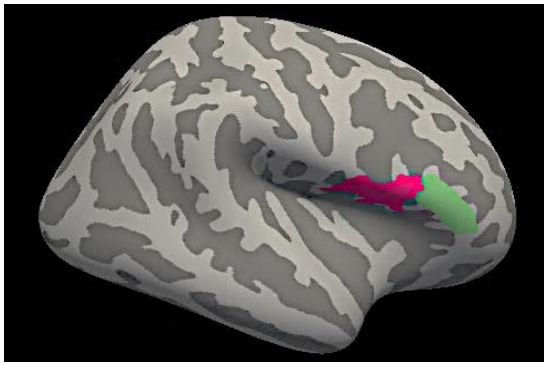

Figure 10. Right pars triangularis (BA44) (green) and pars opercularis (BA45) (magenta) from Destrieux atlas parcellation.